ISSN 0915-633X

NATIONAL INSTITUTE FOR FUSION SCIENCE

Generation of Toroidal Current Sheet at Sawtooth Crash

K. Itoh, S.-I. Itoh, H. Soltwisch and H.R. Koslowski

(Received - Jan. 21, 1997)

NIFS-481 Feb. 1997

RESEARCH REPORT
NIFS Series

NAGOYA, JAPAN

Generation of Toroidal Current Sheet at Sawtooth Crash

K. Itoh*, S.-I. Itoh**, H. Soltwisch†, H. R. Koslowski††

* National Institute for Fusion Science, Nagoya 464-01, Japan
** Research Institute for Applied Mechanics, Kyushu University, Kasuga 816, Japan
† Institute fur Experimentalphysik V, Ruhr Universitat Bochum, D-44801 Bochum, Germany
†† Institut fur Plasmaphysik, Forschungszentrum Julich GmbH, D-52425 Julich, Germany

Abstract

The mechanism to generate the toroidal sheet current after the sawtooth crash (observation on TEXTOR tokamak) is discussed. A possible hypothesis is presented. The crash of central pressure causes the steep gradient near the boundary between the flattened region and the unperturbed region. This sharp pressure gradient gives rise to the strong secondary current (transient Pfirsch-Schluter current). The location, polarity, magnitude and time evolution of the current sheet are analyzed. Comparison with present experimental data is made, and future necessary measurements are discussed.

Keywords: sawtooth crash, toroidal current sheet, TEXTOR tokamak, secondary current

1. Introduction

In the study of the change of the magnetic structure at the onset of sawtooth crash on TEXTOR, the generation of the transient toroidal current has been observed [1, 2]. This transient toroidal current is localized both in the radial and poloidal directions as is illustrated in Fig.1 which is quoted from [3]. The peak of the current is located slightly outside the inversion radius, and the duration time is order of mili-second. The direction of the toroidal sheet current in the outside of the torus is the same as the main plasma current. The direction of the sheet current in the inside of the torus is opposite. That is, the $m = 1 / n = 0$ structure is observed for the transient sheet current, where m and n are the poloidal and toroidal mode numbers, respectively.

The origin of this toroidal current has been conjectured as the shrinkage of the major radius [1]. It is not clear, however, what a mechanism fixes the plasma of the outer region at the original position when the inside plasma shrinks toroidally-inward at the crash. An alternative mechanism to explain the generation of current is discussed in this article. At the onset of the sawtooth crash, the central plasma pressure is flattened, while the outer region is left unchanged. As a result of this, the steep pressure gradient evolves between these two regions. The steep gradient, afterwards, propagates towards the edge; this phenomenon has been known as the heat pulse propagation associated with the sawtooth crash. We analyze the secondary current associated with this steep pressure gradient. It has the m=1/n=0 structure, and is in the same direction as the main plasma current at the outside of the torus. The magnitude and the time evolution of the current sheet are also discussed. Brief comparison with experimental observation is made. Some favourable aspects are obtained, i.e., for the polarity, order of magnitude and the time scale. However, some of experimental features remain unresolved. Possible future experiments are also discussed.

2. Model

The intrinsic feature of the sawtooth crash is that the crash time is much shorter than the energy confinement time, and that the region of the drastic collapse is localized

in the center. Owing to these characteristics, the mesa-shaped pressure profile is established at the end of the crash. The sawtooth crash naturally causes the very steep gradient. The schematic radial profile is drawn in Fig.2. In this figure, the radius r_{KAM} indicates the ridge of the crashed region. The steep pressure gradient is first discussed, and the associated secondary current is calculated accordingly.

The typical time for the crash of the central plasma pressure is denoted by τ_{cr}. This time is much faster than the energy confinement time of the core plasma. For the simplicity, we assume that the energy flux in the outer region, $r > r_{KAM}$, is described by the diffusive transport as

$$\chi = \chi_L \qquad r > r_{KAM} \,, \tag{1}$$

where the suffix L denotes the L-mode confinement. During the crash process, the high heat flux is supplied across the boundary surface, $r = r_{KAM}$, and diffuses in the outer region $r > r_{KAM}$. Due to the very rapid crash time, the heat pulse penetrates only a short distance Δ during the period of τ_{cr}. By use of the diffusion coefficient, χ_L, the layer thickness Δ is evaluated as

$$\Delta \simeq \sqrt{\chi_L \tau_{cr}} \,. \tag{2}$$

If the fast collapse is described by the enhanced transport, as is in the stochasticity model of crash,

$$\chi = \chi_M \qquad r < r_{KAM} \,, \tag{3}$$

the crash time is expressed as $\tau_{cr} = r_1^2 / \chi_M$ where r_1 is the inversion radius. The layer thickness Δ is then expressed as

$$\frac{\Delta}{r_1} \simeq \sqrt{\frac{\chi_L}{\chi_M}} \,. \tag{4}$$

Usually the relation $\chi_M >> \chi_L$ holds, i.e., $\Delta << r_I$.

The steep pressure gradient is estimated as

$$\left|\frac{dp}{dr}\right| = \frac{p_{after}(r_{KAM}) - p_{after}(r_{KAM} + \Delta)}{\Delta}, \tag{5}$$

where the suffix *after* indicates the profile after the crash . Just after the completion of the crash, the profile in the region $r > r_{KAM} + \Delta$ is unaffected. The pressure difference across the region $r_{KAM} < r < r_{KAM} + \Delta$ is given as

$$p_{after}(r_{KAM}) - p_{after}(r_{KAM} + \Delta) \simeq p_f - p_{before}(r_{KAM} + \Delta), \tag{6}$$

where the suffix *before* indicates the profile after the crash and before the crash and p_f stands for the final flat top. The pressure difference is characterized by the initial central value $p(0)$ and p_f. If one assumes a conservation of the average pressure within $r < r_{KAM}$ and if the initial profile in the central region is modelled by the parabolic one, the pressure difference across the thin layer $r_{KAM} < r < r_{KAM} + \Delta$ is given as

$$p_{after}(r_{KAM}) - p_{after}(r_{KAM} + \Delta) \simeq p(0) - p_f . \tag{7}$$

In deriving the estimate (7), we used the limiting approximation of $\Delta << r_I$. Within this assumption, the approximate relation

$$r_{KAM} \simeq \sqrt{2} r_I \tag{8}$$

holds. Note that the assumption of the parabolic profile does not limit the generality of the argument. Based on the estimation Eq.(7), we have the evaluation of the localized pressure gradient, Eq.(5), as

$$\left|\frac{dp}{dr}\right| = \frac{p(0) - p_f}{\Delta} . \qquad (9)$$

Substituting Eq.(4) into Eq.(9), the gradient is evaluated as

$$\left|\frac{dp}{dr}\right| \simeq \frac{p(0) - p_f}{r_1}\sqrt{\frac{\chi_M}{\chi_L}} . \qquad (10)$$

By use of this pressure gradient, the Pfirsch-Schluter current is calculated. This current is mainly in the toroidal direction and has the in-out asymmetry. It is given as

$$J_{\parallel} = -(1 + 2q)\frac{\nabla p}{B}\cos\theta , \qquad (11)$$

where B is the main magnetic field and q is the safety factor [4]. The sign of $J_{\parallel}$ is defined such that it is positive if the current is in the same direction of the main plasma current. Substituting Eq.(10), into Eq.(11), we have

$$J_{\parallel} = (1 + 2q)\sqrt{\frac{\chi_M}{\chi_L}}\,\frac{p(0) - p_f}{B r_1}\cos\theta . \qquad (12)$$

This result indicates that there will appear a localized toroidal current just after the crash of the central pressure. The direction of this induced current is in the same direction as the main plasma current in the outside of the torus ($\theta \simeq 0$) and is opposite to the plasma current at the inside ($\theta \simeq \pi$). It is more convenient to compare, with experiments, the magnitude of the current driven by the sharp pressure gradient. In order to obtain the total current in the current sheet, I_s, we integrate the current density in the region of $-\pi/2 < \theta < \pi/2$ and $r_{KAM} < r < r_{KAM} + \Delta$ as,

$$I_s = \int\int J_{\parallel} d\theta dr . \qquad (13)$$

Substituting Eq.(12) into Eq.(13), the magnitude of the driven current is estimated as

$$I_s = 2(1 + 2q) r_{KAM} \frac{p(0) - p_f}{B} . \qquad (14)$$

At the location of this sheet current, the relation $q \sim 1$ holds. It should be noticed that the expression of current in the sheet, Eq.(14), is independent of the estimate of the layer thickness. The sheet current is given as

$$I_s \simeq 6 r_{KAM} \frac{p(0) - p_f}{B} . \qquad (15)$$

This current could be compared to the total plasma current, I_p, $I_p \simeq 2\pi a^2 B / q(a) \mu_0 R$. Comparing it to Eq.(15), one has

$$\frac{I_s}{I_p} \simeq \frac{3 R r_{KAM}}{2\pi a^2} q(a) \frac{p(0) - p_f}{p(0)} \beta(0) \qquad (16)$$

where $\beta(0) = 2\mu_0 p(0) B^{-2}$. This result suggests that the expected current is large enough to be observed in experiments like those in [1,2].

The sheet current disappears as the steep pressure gradient diffuses away. The typical time scale for the decay of the localized current is given as the heat-pulse-propagation time to the point of the interest. Figure 3 illustrates the schematic drawing of the temporal evolution of the sheet current.

3. Comparison with Experimental Observations

The prediction by the model is compared to the experimental observation.

Polarity is consistent with the observation. The secondary current is in the same direction as the main plasma current at the outside of the torus. The sheet current in the outer mid plane is reported in the direction of the main plasma current [1,2].

Radial thickness of the current layer is given by Eq.(2) or (4). For the typical value of the Ohmic plasma, $\tau_{cr} \simeq 100\mu s$ and $\chi_L \simeq 2m^2/s$, estimation is deduced from

Eq.(2) as $\Delta \simeq 1.4cm$. For the experimental condition in [1,2], the special resolution of the current layer is not yet determined exactly. The peak of the local current is located between two channels of observation, the distance between which is $4.5cm$. If the extrapolation based on the neighbouring channels is employed, the thickness of the current layer seems few cm. The model is not rejected.

Magnitude of the sheet current is given from Eq.(16). For the typical parameters of $n_e(0) = 5 \times 10^{19} m^{-3}$, $T_e = 1keV$, $B = 2T$, $R/a = 3$, $a/r_1 = 3$ and $q(a) = 3$ ($\beta(0) \simeq 0.8\%$), we consider the crash of the magnitude $(p(0) - p_f)/p(0) = 0.1$. Then Eq.(16) provides the estimate $I_s/I_p \sim 0.2\ \%$. The sheet current is of the order of $1kA$. Experimental estimation is reported in [5]. Owing to the uncertainty in the spatial profile of the current, experimental value is not a final one, but a very crude estimate of $I_s \simeq 3kA$ is reported. Order of magnitude may be acceptable, but the conclusion must be made after more detailed measurement will be made.

Poloidal structure is the other key. The formula Eq.(11) only keeps the fundamental $m = 1$ component. This simplification is insufficient. In the experiments [1,2], the strong difference was observed between the inside sheet current and outside one: the sheet current is stronger in the outside and weaker in the inside of the torus. The poloidal localization is estimated to be of the order of $10\ cm$ [4]. The poloidal localization is $20\ cm$ or so after Eq.(11). These observations suggest that the poloidal Fourier components with $m \neq 1$ are also included in the sheet current. This suggests the future necessary improvement in the model.

Temporal dynamics are drawn in Fig.3. At the distance of the observation chord, which is about $3\ cm$ away from the peak of the current, the sheet current is expected to decay within $1\ ms$ with the parameter of $\chi_L \simeq 2m^2/s$. Both the rise time and the decay time are shorter than or of the same magnitude as the time resolution of the measurement, $O(1ms)$.

These comparisons motivate the further experimental observations to test the validity of the present hypothesis.

The poloidal structure can be more precisely observed by use of the horizontal channel. In an experimental set up, which is shown in Fig.4, the transient sheet current can be examined by the horizontal channel. If the even-m Fourier components (such as $m = 0$ component) are associated with the sheet current, the horizontal channel captures the signal. This is one of the key tests for this hypothesis.

Second, the higher time resolution for the Faraday rotation measurement of the vertical codes is desirable. If the time resolution could be improved to the level such as for the present interferometry signal, the rise time and decay time could be precisely determined. The asymmetry is predicted in the rise time and decay time, as is shown in Fig.3, in this hypothesis.

Third, routine observation of the current sheet is necessary. There are varieties in the magnitude of the sawtooth collapse, depending on the plasma operation conditions, e.g., full collapse, partial sawtooth, etc. The correlation between the magnitude of the collapse and the sheet current can then be tested. It will also be fruitful if this measurement of the transient current could be applied to other events, like high-beta collapse or giant ELMs, although such applications would lead to the additional experimental problems and difficulties.

4. Summary

In this note, a hypothesis was discussed on the mechanism to cause the toroidal current sheet at the sawtooth crash. The transient secondary current (transient Pfirsch-Schluter current) is considered to be induced by the steep pressure gradient due to the sawtooth crash. The characteristics of toroidal current sheet are discussed on the aspects of polarity, radial location, thickness of the sheet, poloidal form, magnitude, and temporal evolution. Comparison with the present data is performed. While the hypothesis is not clearly rejected, there are several signs that the improvement of the model is necessary, i.e., poloidal structure. In order to test more precisely, further possible experimental tests are studied. If the correlation between the measured current and the transient secondary current could be confirmed, the experiment on TEXTOR

would provide the first direct experimental observation of the secondary current in toroidal plasmas. It would explore a fundamental basis for the understanding of toroidal plasmas. Further experiments are motivated.

Several improvements of the model may be possible. For instance, in the presence of the steep gradient, the Shafranov shift could also be important. Owing to the Shafranov shift, the pressure gradient, and hence the driven current as well, are increased in the outside of the torus and are reduced in the inside of the torus. This effect could yield an in-out asymmetry: Such corrections must be taken into account is a systematic way, and await future careful work.

The hypothesis of the generation mechanism for the sheet current, which is discussed here, is not a consequence of a particular model of the sawtooth crash. This hypothesis is based on the rapid and localized crash of the sawtooth and on the fact that the q-profile changes little after the crash [6]. The relevance of the sawtooth models, e.g., the stochasticity model [7], the large convection model [8] or localized reconnection model [9], could be examined by the comparison with the experimental observation on the helical magnetic perturbations [5, 10].

Acknowledgements

This work is performed under the Japan-TEXTOR collaboration programme. Authors acknowledge Prof. G. H. Wolf and Prof. T. Kuroda for the support of the programme. They also wish to thank Prof. N. Noda for continuous help and arrangements. Two of the authors (KI and SII) are grateful to the support of Prof. K. N. Sato. This work is partly supported by the Grant-in-Aid for Scientific Research of MoE Japan, by the collaboration programme of NIFS and by the collaboration programme of Advanced research Center of Kyushu University.

References

[1] Soltwisch H, Fuchs G, Koslowski H R, Schlueter J, Waidmann G 1991 *Proc. 18th Eur. Conf. on Controlled Fusion and Plasma Physics, Berlin*, Europhys. Conf. Abstr., Vol.15C, Part-II, 17 (Eur. Phys. Soc. Geneva).

[2] Soltwisch H, Koslowski H R 1995 *Plasma Phys. Contr. Fusion* **37** 667.

[3] Soltwisch H 1994 in *Contributions to High Temperature Plasma Physics* (Akademie Verlag, Berlin) ed. K. H. Spatschek and J. Uhlenbusch, p.471.

[4] Miyamoto K 1976 *Plasma Physics for Nuclear Fusion* (2nd ed., Iwanami, Tokyo) Chap. 7.8.

[5] Soltwisch H, Koslowski H R 1996 "*Observation of magnetic field perturbations during sawtooth activity in tokamak plasmas*", presented at the *International Conf. Plasma Phys.* (Nagoya).

[6] Soltwisch H, Stodiek W, Manickam J, Schlueter J 1986 *Plasma Physics and Controlled Nuclear Fusion Research 1986* (IAEA, Vienna) Vol.1, 263.

[7] Lichtenberg A J, Itoh K, Itoh S-I, Fukuyama A 1992 *Nucl. Fusion* **32** 495.

[8] Biskamp D, Drake J F 1994 *Phys. Rev. Lett.* **73** 971
Naitou H, Tsuda K, Lee W W, Sydora R D 1995 *Phys. Plasmas* **2** 4257.

[9] Nagayama Y, et al. 1996 *Phys. Plasmas* **3** 1647.

[10] Koslowski H R, Soltwisch H 1995 *Plasma Phys. Contr. Fusion* **38** 271.

Figure Captions

Fig. 1 Plasma torus with axisymmetric toroidal current sheets. (Quoted From [3].) The outer sheet carries the current in the same direction as the main plasma current. The inner sheet current directs to the opposite.

Fig.2 Pressure profile after the crash (solid line) and before the crash (dashed line).

Fig.3 Schematic drawing for time evolution of the sheet current.

Fig.4 Poloidal cross section of the experimental set up. By use of the bottom limiter, the line of the sight of the horizontal channel is arranged near the radius of interest. The central hatched circle indicates the region where collapse takes place.

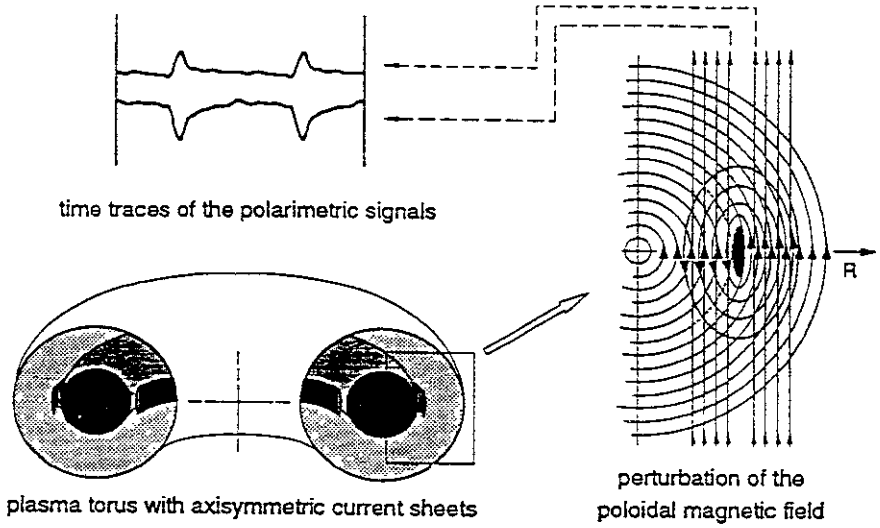
time traces of the polarimetric signals
R
plasma torus with axisymmetric current sheets
perturbation of the
poloidal magnetic field

Fig.1

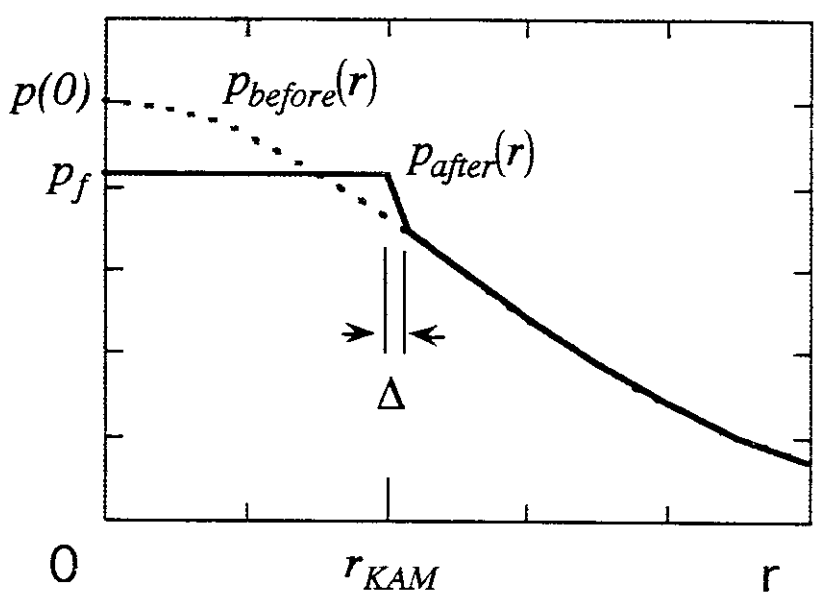
p(0)
$p_{before}(r)$
$p_{after}(r)$
p_f
Δ
0
r_{KAM}
r

Fig.2

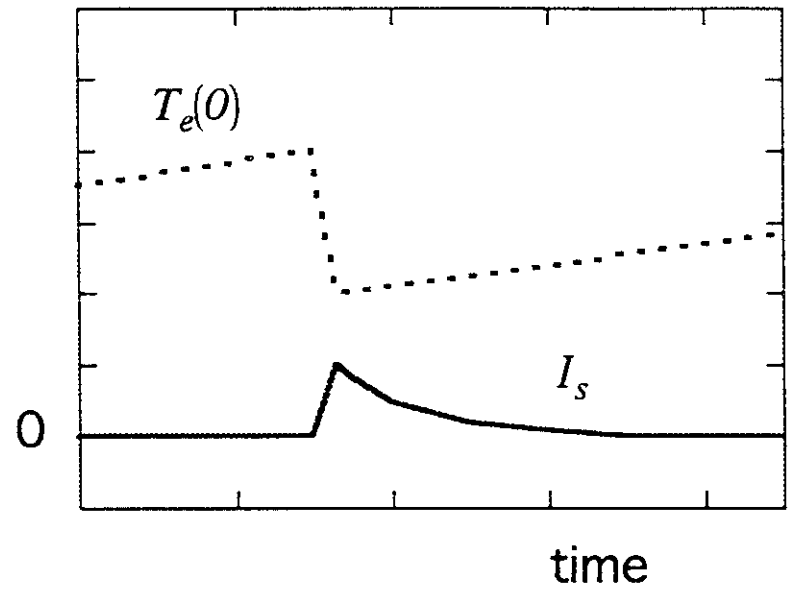

Fig.3

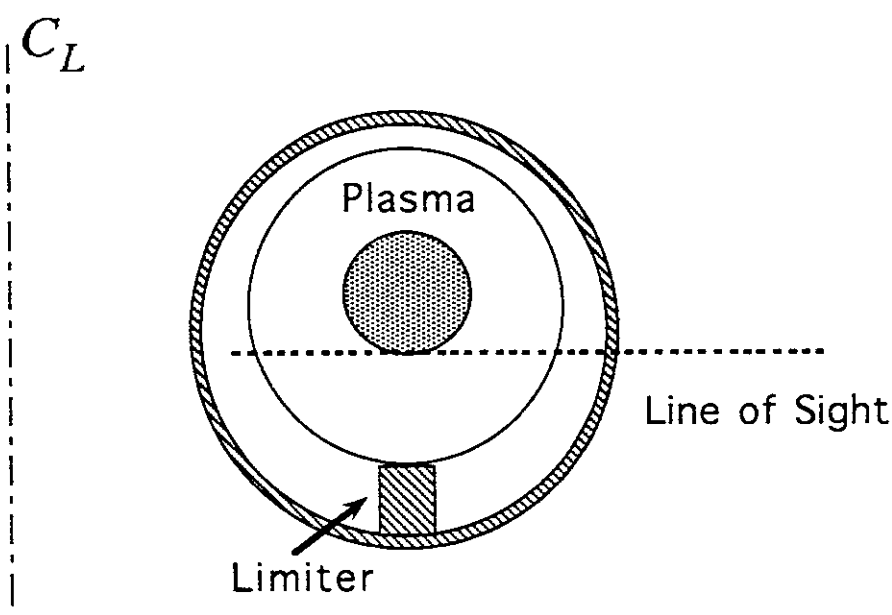

Fig.4

Recent Issues of NIFS Series

NIFS-440 S. Morita, H. Idei, H. Iguchi, S. Kubo, K. Matsuoka, T. Minami, S. Okamura, T Ozaki, K. Tanaka, K. Toi, R. Akiyama, A. Ejiri, A. Fujisawa, M. Fujiwara, M. Goto, K. Ida, N. Inoue, A. Komori, R Kumazawa, S. Masuzaki, T. Morisaki, S. Muto, K. Narihara, K. Nishimura, I. Nomura, S. Ohdachi, M.. Osakabe, A. Sagara, Y. Shirai, H. Suzuki, C. Takahashi, K. Tsumori, T. Watari, H. Yamada and I. Yamada,
A Study on Density Profile and Density Limit of NBI Plasmas in CHS: Sep. 1996 (IAEA-CN-64/CP-3)

NIFS-441 O. Kaneko, Y. Takeiri, K. Tsumori, Y. Oka, M. Osakabe, R. Akiyama, T. Kawamoto, E. Asano and T. Kuroda,
Development of Negative-Ion-Based Neutral Beam Injector for the Large Helical Device; Sep. 1996 (IAEA-CN-64/GP-9)

NIFS-442 K. Toi, K.N. Sato, Y. Hamada, S. Ohdachi, H. Sakakita, A. Nishizawa, A. Ejiri, K. Narihara, H. Kuramoto, Y. Kawasumi, S. Kubo, T. Seki, K. Kitachi, J. Xu, K. Ida, K. Kawahata, I. Nomura, K. Adachi, R. Akiyama, A. Fujisawa, J. Fujita, N. Hiraki, S. Hidekuma, S. Hirokura, H. Idei, T. Ido, H. Iguchi, K. Iwasaki, M. Isobe, O. Kaneko, Y. Kano, M. Kojima, J. Koog, R. Kumazawa, T. Kuroda, J. Li, R. Liang, T. Minami, S. Morita, K. Ohkubo, Y. Oka, S. Okajima, M. Osakabe, Y. Sakawa, M. Sasao, K. Sato, T. Shimpo, T. Shoji, H. Sugai, T. Watari, I. Yamada and K. Yamauti,
Studies of Perturbative Plasma Transport, Ice Pellet Ablation and Sawtooth Phenomena in the JIPP T-IIU Tokamak; Sep. 1996 (IAEA-CN-64/A6-5)

NIFS-443 Y. Todo, T. Sato and The Complexity Simulation Group,
Vlasov-MHD and Particle-MHD Simulations of the Toroidal Alfvén Eigenmode; Sep. 1996 (IAEA-CN-64/D2-3)

NIFS-444 A. Fujisawa, S. Kubo, H. Iguchi, H. Idei, T. Minami, H. Sanuki, K. Itoh, S. Okamura, K. Matsuoka, K. Tanaka, S. Lee, M. Kojima, T.P. Crowley, Y. Hamada, M. Iwase, H. Nagasaki, H. Suzuki, N. Inoue, R. Akiyama, M. Osakabe, S. Morita, C. Takahashi, S. Muto, A. Ejiri, K. Ida, S. Nishimura, K. Narihara, I. Yamada, K. Toi, S. Ohdachi, T. Ozaki, A. Komori, K. Nishimura, S. Hidekuma, K. Ohkubo, D.A. Rasmussen, J.B. Wilgen, M. Murakami, T. Watari and M. Fujiwara,
An Experimental Study of Plasma Confinement and Heating Efficiency through the Potential Profile Measurements with a Heavy Ion Beam Probe in the Compact Helical System; Sep. 1996 (IAEA-CN-64/C1-5)

NIFS-445 O. Motojima, N. Yanagi, S. Imagawa, K. Takahata, S. Yamada, A. Iwamoto, H. Chikaraishi, S. Kitagawa, R. Maekawa, S. Masuzaki, T. Mito, T. Morisaki, A. Nishimura, S. Sakakibara, S. Satoh, T. Satow, H. Tamura, S. Tanahashi, K. Watanabe, S. Yamaguchi, J. Yamamoto, M.Fujiwara and A. Iiyoshi,
Superconducting Magnet Design and Construction of LHD; Sep. 1996 (IAEA-CN-64/G2-4)

NIFS-446 S. Murakami, N. Nakajima, S. Okamura, M. Okamoto and U. Gasparino,

Orbit Effects of Energetic Particles on the Reachable β–Value and the Radial Electric Field in NBI and ECR Heated Heliotron Plasmas; Sep. 1996 (IAEA-CN-64/CP -6) Sep. 1996

NIFS-447 K. Yamazaki, A. Sagara, O. Motojima, M. Fujiwara, T. Amano, H. Chikaraishi, S. Imagawa, T. Muroga, N. Noda, N. Ohyabu, T. Satow, J.F. Wang, K.Y. Watanabe, J. Yamamoto , H. Yamanishi, A. Kohyama, H. Matsui, O. Mitarai, T. Noda, A.A. Shishkin, S. Tanaka and T. Terai
Design Assessment of Heliotron Reactor; Sep. 1996 (IAEA-CN-64/G1-5)

NIFS-448 M. Ozaki, T. Sato and the Complexity Simulation Group,
Interactions of Convecting Magnetic Loops and Arcades; Sep. 1996

NIFS-449 T. Aoki,
Interpolated Differential Operator (IDO) Scheme for Solving Partial Differential Equations; Sep. 1996

NIFS-450 D. Biskamp and T. Sato,
Partial Reconnection in the Sawtooth Collapse; Sep. 1996

NIFS-451 J. Li, X. Gong, L. Luo, F.X. Yin, N. Noda, B. Wan, W. Xu, X. Gao, F. Yin, J.G. Jiang, Z. Wu., J.Y. Zhao, M. Wu, S. Liu and Y. Han,
Effects of High Z Probe on Plasma Behavior in HT-6M Tokamak; Sep. 1996

NIFS-452 N. Nakajima, K. Ichiguchi, M. Okamoto and R.L. Dewar,
Ballooning Modes in Heliotrons/Torsatrons; Sep. 1996 (IAEA-CN-64/D3-6)

NIFS-453 A. Iiyoshi,
Overview of Helical Systems; Sep. 1996 (IAEA-CN-64/O1-7)

NIFS-454 S. Saito, Y. Nomura, K. Hirose and Y.H. Ichikawa,
Separatrix Reconnection and Periodic Orbit Annihilation in the Harper Map; Oct. 1996

NIFS-455 K. Ichiguchi, N. Nakajima and M. Okamoto,
Topics on MHD Equilibrium and Stability in Heliotron / Torsatron; Oct. 1996

NIFS-456 G. Kawahara, S. Kida, M. Tanaka and S. Yanase,
Wrap, Tilt and Stretch of Vorticity Lines around a Strong Straight Vortex Tube in a Simple Shear Flow; Oct. 1996

NIFS-457 K. Itoh, S.- I. Itoh, A. Fukuyama and M. Yagi,
Turbulent Transport and Structural Transition in Confined Plasmas; Oct. 1996

NIFS-458 A. Kageyama and T. Sato,
Generation Mechanism of a Dipole Field by a Magnetohydrodynamic Dynamo; Oct. 1996

NIFS-459 K. Araki, J. Mizushima and S. Yanase,
The Non-axisymmetric Instability of the Wide-Gap Spherical Couette Flow; Oct. 1996

NIFS-460 Y. Hamada, A. Fujisawa, H. Iguchi, A. Nishizawa and Y. Kawasumi,
A Tandem Parallel Plate Analyzer; Nov. 1996

NIFS-461 Y. Hamada, A. Nishizawa, Y. Kawasumi, A. Fujisawa, K. Narihara, K. Ida, A. Ejiri, S. Ohdachi, K. Kawahata, K. Toi, K. Sato, T. Seki, H. Iguchi, K. Adachi, S. Hidekuma, S.Hirokura, K. Iwasaki, T. Ido, M. Kojima, J. Koong, R. Kumazawa, H. Kuramoto, T. Minami, I. Nomura, H. Sakakita, M. Sasao, K.N. Sato, T. Tsuzuki, J. Xu, I. Yamada and T. Watari,
Density Fluctuation in JIPP T-IIU Tokamak Plasmas Measured by a Heavy Ion Beam Probe; Nov. 1996

NIFS-462 N. Katsuragawa, H. Hojo and A. Mase,
Simulation Study on Cross Polarization Scattering of Ultrashort-Pulse Electromagnetic Waves; Nov. 1996

NIFS-463 V. Voitsenya, V. Konovalov, O. Motojima, K. Narihara, M. Becker and B. Schunke,
Evaluations of Different Metals for Manufacturing Mirrors of Thomson Scattering System for the LHD Divertor Plasma; Nov. 1996

NIFS-464 M. Pereyaslavets, M. Sato, T. Shimozuma, Y. Takita, H. Idei, S. Kubo, K. Ohkubo and K. Hayashi,
Development and Simulation of RF Components for High Power Millimeter Wave Gyrotrons; Nov. 1996

NIFS-465 V.S. Voitsenya, S. Masuzaki, O. Motojima, N. Noda and N. Ohyabu,
On the Use of CX Atom Analyzer for Study Characteristics of Ion Component in a LHD Divertor Plasma; Dec. 1996

NIFS-466 H. Miura and S. Kida,
Identification of Tubular Vortices in Complex Flows; Dec. 1996

NIFS-467 Y. Takeiri, Y. Oka, M. Osakabe, K. Tsumori, O. Kaneko, T. Takanashi, E. Asano, T. Kawamoto, R. Akiyama and T. Kuroda,
Suppression of Accelerated Electrons in a High-current Large Negative Ion Source; Dec. 1996

NIFS-468 A. Sagara, Y. Hasegawa, K. Tsuzuki, N. Inoue, H. Suzuki, T. Morisaki, N. Noda, O. Motojima, S. Okamura, K. Matsuoka, R. Akiyama, K. Ida, H. Idei, K. Iwasaki, S. Kubo, T. Minami, S. Morita, K. Narihara, T. Ozaki, K. Sato, C. Takahashi, K. Tanaka, K. Toi and I. Yamada,
Real Time Boronization Experiments in CHS and Scaling for LHD; Dec. 1996

NIFS-469 V.L. Vdovin, T.Watari and A. Fukuyama,
3D Maxwell-Vlasov Boundary Value Problem Solution in Stellarator

Geometry in Ion Cyclotron Frequency Range (final report); Dec. 1996

NIFS-470 N. Nakajima, M. Yokoyama, M. Okamoto and J. Nührenberg,
Optimization of M=2 Stellarator; Dec. 1996

NIFS-471 A. Fujisawa, H. Iguchi, S. Lee and Y. Hamada,
Effects of Horizontal Injection Angle Displacements on Energy Measurements with Parallel Plate Energy Analyzer; Dec. 1996

NIFS-472 R. Kanno, N. Nakajima, H. Sugama, M. Okamoto and Y. Ogawa,
Effects of Finite-β and Radial Electric Fields on Neoclassical Transport in the Large Helical Device; Jan. 1997

NIFS-473 S. Murakami, N. Nakajima, U. Gasparino and M. Okamoto,
Simulation Study of Radial Electric Field in CHS and LHD; Jan. 1997

NIFS-474 K. Ohkubo, S. Kubo, H. Idei, M. Sato, T. Shimozuma and Y. Takita,
Coupling of Tilting Gaussian Beam with Hybrid Mode in the Corrugated Waveguide; Jan. 1997

NIFS-475 A. Fujisawa, H. Iguchi, S. Lee and Y. Hamada,
Consideration of Fluctuation in Secondary Beam Intensity of Heavy Ion Beam Prove Measurements; Jan. 1997

NIFS-476 Y. Takeiri, M. Osakabe, Y. Oka, K. Tsumori, O. Kaneko, T. Takanashi, E. Asano, T. Kawamoto, R. Akiyama and T. Kuroda,
Long-pulse Operation of a Cesium-Seeded High-Current Large Negative Ion Source; Jan. 1997

NIFS-477 H. Kuramoto, K. Toi, N. Haraki, K. Sato, J. Xu, A. Ejiri, K. Narihara, T. Seki. S. Ohdachi, K. Adati, R. Akiyama, Y. Hamada, S. Hirokura, K. Kawahata and M. Kojima,
Study of Toroidal Current Penetration during Current Ramp in JIPP T-IIU with Fast Response Zeeman Polarimeter; Jan. 7, 1997

NIFS-478 H. Sugama and W. Horton,
Neoclassical Electron and Ion Transport in Toroidally Rotating Plasmas; Jan. 1997

NIFS-479 V.L. Vdovin and I.V. Kamenskij,
3D Electromagnetic Theory of ICRF Multi Port Multi Loop Antenna; Jan. 1997

NIFS-480 W.X. Wang, M. Okamoto, N. Nakajima, S Murakami and N. Ohyabu,
Cooling Effect of Secondary Electrons in the High Temperature Divertor Operation; Feb. 1997

NIFS-481 K. Itoh, S.-I. Itoh, H. Soltwisch and H.R. Koslowski,
Generation of Toroidal Current Sheet at Sawtooth Crash; Feb. 1997